ACS APPLIED MATERIALS & INTERFACES

Research Article

www.acsami.org

Nitrogen-Doped Hierarchical Lamellar Porous Carbon Synthesized from the Fish Scale As Support Material for Platinum Nanoparticle Electrocatalyst toward the Oxygen Reduction Reaction

Haijing Liu,[†] Yinliang Cao,[†] Feng Wang,* and Yaqin Huang*

State Key Laboratory of Chemical Resource Engineering, Beijing Key Laboratory of Electrochemical Process and Technology for Materials, Beijing University of Chemical Technology, Beijing 100029, P. R. China

ABSTRACT: Novel hierarchical lamellar porous carbon (HLPC) with high BET specific surface area of 2730 m^2 g^{-1} and doped by nitrogen atoms has been synthesized from the fish scale without any post-synthesis treatment, and applied to support the platinum (Pt) nanoparticle (NP) catalysts (Pt/HLPC). The Pt NPs could be highly dispersed on the porous surface of HLPC with a narrow size distribution centered at ca. 2.0 nm. The results of the electrochemical analysis reveal that the electrochemical active surface area (ECSA) of Pt/HLPC is larger than the Pt NP electrocatalyst supported on the carbon black (Pt/Vulcan XC-72). Compared with the Pt/Vulcan XC-72, the Pt/HLPC exhibits larger current density, lower overpotential, and enhanced catalytic activity toward the oxygen reduction reaction (ORR) through the direct four-electron pathway. The improved catalytic activity is mainly attributed to the high BET specific surface area, hierarchical porous structures and the nitrogen-doped surface property of HLPC, indicating the superiority of HLPC as a promising support material for the ORR electrocatalysts.

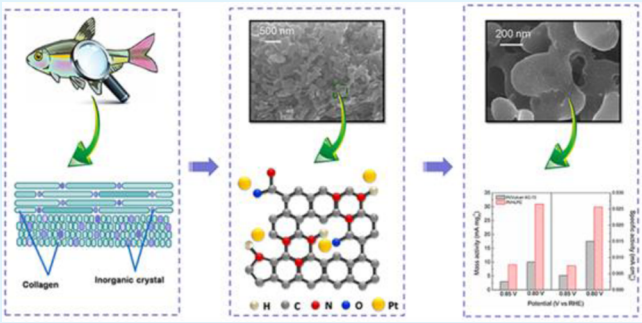

KEYWORDS: *oxygen reduction reaction, hierarchical lamellar porous carbon, nanoparticle, electrocatalyst, fish scale*

1. INTRODUCTION

Because of the high efficiency, low operating temperature, simple processing, and possibility of portable electrical applications,[1] polymer electrolyte membrane fuel cell (PEMFC) is considered as one of the most promising candidates for the power generation. Despite these advantages, there are several obstacles in preventing the commercialization of PEMFC, such as durability under long-term operation[2] and high cost of platinum (Pt) electrocatalysts, which is well accepted as the best commercial catalyst for the cathodic oxygen reduction reaction (ORR) and anodic hydrogen oxidation reaction (HOR).[3] Considering that the cathode ORR is six or more orders of magnitude slower than the anode HOR, thus limiting the total efficiency of PEMFC,[4] there has been intensive research effort to improve the ORR kinetics, focused on developing more active and high efficient electrocatalysts for the ORR process with significantly lower Pt content by applying the alloys of Pt and transition metals, such as Fe, Co, or Ni,[5−7] or the design and synthesis of new carbon support materials for electrocatalysts.[8]

A well-designed support material for the electrocatalysts toward the ORR process should acquire certain kinds of characteristics, such as suitable specific surface area and surface chemistry, high stability, high conductivity, as well as an accessible porosity.[9] According to these principles, the balance among the conductivity, specific surface area and cost[10] enable the carbon black, such as Vulcan XC-72, to be a highly favored support material for the commercial ORR electrocatalysts. However, there are still some disadvantages unsolved as the stability. As is known to all, the ORR often proceeds at the high overpotential in a corrosive solution, but the Vulcan XC-72 applied as the support material for electrocatalyst is not stable at such harsh environment, thus negatively affecting the activity of the supported electrocatalysts.[11] Several novel carbon materials, such as carbon nanotubes,[12] carbon nanofibers,[13] and carbon hollows,[14] are now investigated as the support materials in order to improve the stability and catalytic properties, but they exhibit poor pore structures, low surface area and lack of surface functional groups, that need to be pre-modified by the physical or chemical treatment.[15,16] Considering that the porosity and high specific surface area can improve the affinity between the reactant species and the electrocatalysts, which allows the electrochemical reactions to take place,[17] carbon materials with various porous structures such as mesoporous carbons[18] have been employed as some promising support materials for the electrocatalysts in order to obtain efficient mass transfer of reactants during the ORR process. Recently, functionalizing carbon materials with nitrogen containing groups or incorporation of nitrogen atoms with carbon frameworks have been proved to highly promote the

Received: August 19, 2013
Accepted: December 23, 2013
Published: December 23, 2013

activity of the electrocatalyst. However, the nitrogen doping is mainly obtained by complicated post-synthesis treatment such as long time reaction with ammonium hydroxide or carbonization with nitrogen-contained polymers.[19] Consequently, for the purpose of simultaneously improving the mass transport, dispersion, and stability of electrocatalysts, one of the most important issue corresponding to the PEMFCs is addressed at developing new carbon support materials simultaneously with suitable porous structure and nitrogen-containing functional groups, which can promote the elelctrochemical performance of the electrocatalysts. Obviously, it is still a challenge finding an easy route to fulfill the above objective.

Herein, a novel hierarchical lamellar porous carbon (HLPC) doped by nitrogen atoms was synthesized from the fish scales without any post-synthesis treatment.[20] The HLPC with interconnected porous structure, high surface area, and numerous nitrogen atoms was applied as the support material for the Pt nanoparticle (NP) electrocatalysts (Pt/HLPC) by the ethylene glycol reduction method,[21,22] which has been recognized as a simple method to obtain the well-dispersed Pt NPs with tunable particle size supported on support materials. The resulting Pt NPs can be highly dispersed on the surface of HLPC with a narrow particle size distribution centered at 2.0 nm. The electrochemical performances of the Pt/HLPC were evaluated against commercial carbon black supported Pt NP electrocatalysts, which is referred as the Pt/Vulcan XC-72, prepared under the similar conditions.

2. EXPERIMENTAL SECTION

2.1. Synthesis and Characterization of Materials. The preparation method of the HLPC was similar to the reported one by our group,[20] but the fish scale as the precursor was obtained from Tilapia mossambica, which is different from that used in the previous work. The fish scale was pre-carbonized at 330 °C for 3 h under the air atmosphere. Then the samples were mixed with KOH and then heated in a nitrogen atmosphere at 950 °C for 1 h. The resulting HLPC was washed and kept at 120 °C under vacuum for 24 h.

The Pt NPs were deposited using ethylene glycol as the reducing agent. The support materials (30 mg) were mixed in a 250 mL three-necked flask with the ethylene glycol (100 mL) by sonicating for 30 min, followed by adding 4.61 mL of hexacholoroplatinic acid/ethylene glycol (0.01 mol L^{-1}) solution. The above solution was constantly stirred under refluxing for 3 h at 130 °C after adjusting the pH value to 10. The obtained samples were washed with deionized water for several times, and then kept in a vacuum oven at 80 °C for 24 h. For comparison, Pt loaded on Vulcan XC-72 (commercial carbon black) was fabricated using the same method. The loading rates of Pt NPs on both the HLPC and Vulcan XC-72 were 20 wt %.

The surface morphology was characterized by the field-emission scanning electron microscopy (FE-SEM) conducted on a JEOL JSM-6701 operating at 15 KV. Transmission electron microscopy (TEM) was carried out at JEOL JSM-2100 microscopy (acceleration voltage: 200 kV). The X-ray photoelectron spectroscopy (XPS) results was obtained on the instrument of ESCALAB 250, and C 1s (284.6 eV) was used as a reference for binding energy. Fourier transform infrared spectroscopy (FT-IR) was measured by a PerkinElmer Spectrum 100 from KBr pellets. Nitrogen absorption isotherm was measured on Quantachrome AUTOSORB-1. Prior to the measurement, the samples were degassed at 423 K for 12 h. Powder X-ray diffraction (XRD) measurement was carried out on the Rigaku D/max-2500 with a Cu Kα (α = 1.54 Å).

2.2. Electrochemical Measurements. Electrochemical measurements were conducted in a three-electrode system using a glassy carbon rotating disk electrode (RDE, Pine Research Instrumentation) connected to a PARSTAT 283 potentialstat (Princeton Applied Research). A Pt wire was used as the counter electrode. The reference electrode was a saturated calomel electrode (SCE), and all the potentials mentioned in this article were converted to values with reference to a reversible hydrogen electrode (RHE). Five milligrams of the electrocatalysts were dispersed in the mixture of ethanol (1 mL) and Nafion solution (5 wt %, 50 μL) (DuPont, USA), and then 0.009 mL of the mixture was transferred to the surface of the freshly polished RDE applying as the working electrode. The mass amount of electrocatalysts loaded on the carbon glassy carbon electrodes was 0.045 mg, and the mass amount of Pt NPs could be calculated as 0.009 mg according to the loading rate of the electrocatalysts (20.0 Pt wt.%). The electrochemical experiments, including the cyclic voltammetry and linear polarization were performed at 30 °C. The current densities were normalized to the geometric surface area of the electrode (0.2472 cm^2).

3. RESULTS AND DISCUSSION

As seen in Figure 1, the HLPC exhibits a three-dimensional (3D) hierarchical lamellar porous structure, and well-developed

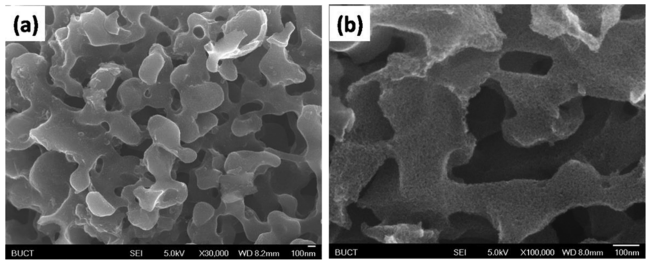

Figure 1. FE-SEM images of the HLPC at (a) low magnification and (b) high magnification.

open macropores interconnected with each other, whose pore size varies from 0.5 μm to 2 μm. Such unique structure of the HLPC derived from the sintering of collagen fibers by using inorganic components served as hard template and collagen fibers served as carbon source as well as soft template in the fish scale.[20] The interconnected pores yield high surface area and provide access to the pores for subsequent filling with a second component,[23] as well as the ion transport pathway through the carbon walls during the mass transportation process.[24]

XPS was conducted in order to analyze the chemical composition and the surface chemical state of the obtained HLPC. It can be observed from Figure 2a that the HLPC exhibits peaks corresponding to the C 1s, N 1s and O 1s, indicating the existence of nitrogen element. The surface atom composition ratio among C, N, O elements is C:N:O = 80.2:9.0:10.8. The high-resolution spectrum of the N 1s peaks showed in Figure 2b suggests the presence of sp^3 hybrid pyrrolic N (400.3 eV) and sp^2 hybrid quaternary N (401.4 eV)[24] on the surface of HLPC. Some of the nitrogen atoms from the proteoglycan of the fish scale insert into the carbon framework to form the pyrrolic-like structures mainly through the defects of aromatic rings during the carbonization.[25] This process is similar to the synthesis of nitrogen-doped porous carbon and carbon nanotubes[26] but talking place simultaneously with carbonization process of fish scales, leading to the potential enhanced electrocatalytic activity for the ORR process.[25,26] The structures were further analyzed by the FI-IR spectrum, and the result was shown in Figure 3. The 1640 cm^{-1} band is corresponding to the C═O vibration of carboxylic groups and the 1255 cm^{-1} band is due to the C−O stretching.[27] Together with the band centered in the range of 1062-1101 cm^{-1} which is assigned to the C−C−O structure,[28] the results above indicate the presence of oxygen in the form of

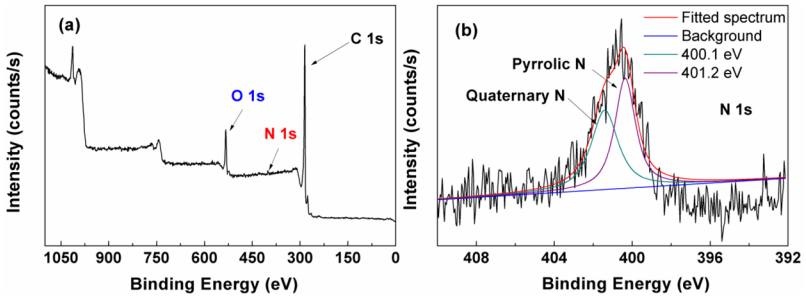

Figure 2. XPS spectra of the HLPC derived from the fish scale: (a) wide scan, (b) N 1s.

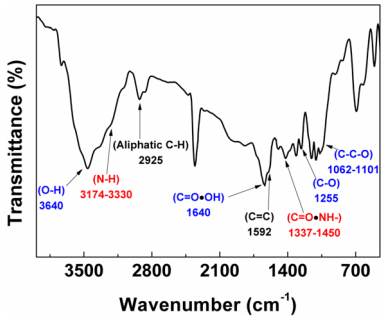

Figure 3. FT-IR spectra of the HLPC derived from fish scales.

carboxyl-groups and carbonyl-groups. The bands in the range of 3174−3330 cm^{-1} that are partly overlapped by the O−H stretching are assigned to N−H stretching, and the bands around 1337−1450 cm^{-1} are corresponding to C═O vibration of amides.[28] The results further proved that presence of nitrogen atoms incorporated into graphite and quaternary nitrogen atoms with amide groups and amino groups.

The porosity and specific surface area of HLPC were characterized by the nitrogen adsorption and desorption isotherms and the results are presented in Figure 4 together with the pore size distribution for the micropores calculated by the Horvanth−Kawazoe (HK) method and mesopores calculated by the Barrett−Joyner−Halenda (BJH) method. As shown in Figure 4a, the N_2 absorption-desorption isotherm is close to a combination form of type I and type IV according to the IPUAC classification. The corresponding BJH mesopore size distribution indicates the pore sizes are mainly between 2−4 nm and the size distribution is quite narrow with a maximum at 3.4 nm, while there is a relatively broad distribution of the micropores in the range of 0.4−2 nm with a sharp maximum at 0.56 nm. The specific Brunauer−Emmett−Teller (BET) calculated from the absorption branch reaches as high as 2730 m^2 g^{-1}, which is much larger than the previous report about porous carbon derived from some other biometerials.[29] On the basis of the analysis of N_2 sorption measurement, the HLPC not only possesses high specific surface area but also has well-developed porosity ranging from micro- to macrocales. The carbonization and activation processes create large amounts of meso- and micropores without destroying the lamellar structure of initial fish scales.

Figure 5 exhibits the SEM and TEM images, selected area electron diffraction (SAED) pattern, and histogram of particle

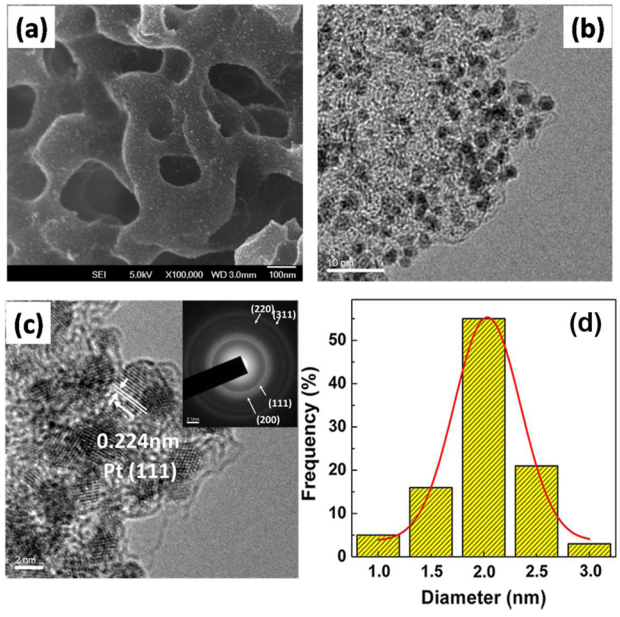

Figure 5. (a) SEM image of the Pt/HLPC; (b, c) TEM images of the Pt/HLPC; inset to c, SAED image of the Pt/HLPC; (d) histogram of the particle size distribution.

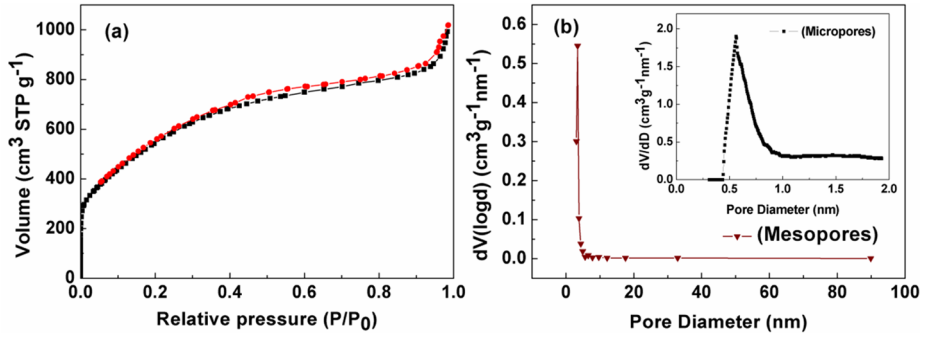

Figure 4. (a) N_2 adsorption/desorption isotherms and (b) the corresponding pore-size distribution curves of the HLPC derived from the fish scale.

dx.doi.org/10.1021/am403432h | ACS Appl. Mater. Interfaces 2014, 6, 819−825

size distribution of the Pt/HLPC. After the chemical reduction, the Pt NPs can be uniformly dispersed on the surface of HLPC (Figure 5a, b), and the hierarchical lamellar structure of the HLPC is remained after depositing the Pt NPs. The d-spacing corresponding to the (111) plane is 0.224 nm measured from HR-TEM image. The four diffraction rings observed from SAED patterns (Figure 5c inset) are assigned to the (111), (200), (220), and (311) planes for the face-centered cubic (fcc) structure of the Pt NPs.[30] The distribution of the particle diameters is calculated from 100 particles, and the result indicates a homogeneous particle size distribution from 1−3 nm with an average diameter of 2.0 nm. The small particle size and uniform diameter distributions of the Pt NPs are mainly attributed to the high specific BET surface area and functionalized surface state of the HLPC.

Figure 6 shows the XRD patterns of the Pt/HLPC and Pt/Vulcan X-72. The patterns exhibit a rather wide and shallow

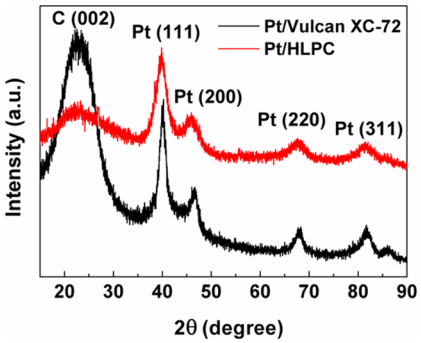

Figure 6. XRD patterns of the Pt/HLPC and Pt/Vulcan X-72.

(002) peak around 23°, implying that the support materials are amorphous carbons with small regions of crystalline. The four peaks from both catalysts centered at 39.8, 46.2, 67.7, and 81.4° are assigned to the (111), (200), (220), and (311) planes of fcc structure of Pt (JCPDS-ICDD, card No. 04-802), respectively. The crystalline size of the Pt NPs supported on the HLPC and Vulcan XC-72 estimated by Scherrer's equation from (111) planes is 2.2 and 3.4 nm, respectively, suggesting a smaller average particle size for the Pt/HLPC. The d-spacing of (111) plane from the Pt/HLPC calculated from Bragg formula is 0.224 nm, which are in accordance with the SAED results.

In order to determine the electrochemical active surface area (ECSA), the cyclic voltammograms (CV) of Pt/HLPC and Pt/Vulcan XC-72 catalysts (Figure 7) were scanned from 0.018 to

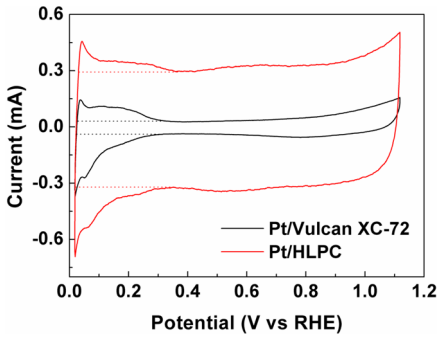

Figure 7. Cyclic voltammograms of the Pt/HLPC and Pt/Vulcan XC-72 scanned in 0.5 mol L^{-1} H_2SO_4 solution at the scan rate of 50 mV s^{-1}.

1.118 V (vs. RHE) at the scanning rate of 50 mV s^{-1} in N_2 saturated 0.5 mol L^{-1} H_2SO_4 solutions. Observed from the the CV curves (Figure 7), two distinctive potential ranges corresponding to the underpotentially deposited hydrogen adsorption/desorption process ($H^+ + e^- = H_{upd}$, $0.018 < E < 0.37$ V) and the formation of a adsorbed hydroxyl species layer ($2H_2O = OH_{ad} + H_3O^+ + e^-$, >0.6 V), respectively.[31] The ECSA of Pt/HLPC and Pt/Vulcan XC-72 can be calculated from the charge required for the hydrogen adsorption/desorption (Q_H) after double-layer correction.[32]

$$\mathrm{ECSA} = Q_H/(0.21[\mathrm{Pt}]) \quad (1)$$

where [Pt] is mass loading rate (mg cm^{-2}) of the Pt NPs on the electrode, Q_H is the charge for hydrogen adsorption/desorption (mC cm^{-2}), and 0.21 represents the charge required to oxidize a monolayer of hydrogen.[33] Considering the asymmetry of the hydrogen adsorption and desorption peaks, the value of Q_H can be calculated by only adsorption peak[34]/desorption peak,[35] or taking the mean value between the charges of these two peaks.[36,37] According to the calculation, the ECSA of Pt/HLPC is 120.7 m^2 g^{-1}, almost two times larger than the Pt/Vulcan XC-72 (66.7 m^2 g^{-1}), suggesting higher utilization of the Pt NPs supported on the HLPC induced by the open macroporous structure and nitrogen atoms.[38] In this case, the Pt NPs deposit on the nitrogen-doped sites exposed larger catalytic active areas than those in the micropores of the HLPC comparing with Pt NPs deposited on several highly porous carbon materials as support materials for electrocatalyst,[39] thus leading to the smaller particle size and lower degree of aggregation of Pt NPs on HLPC.

The kinetic parameters refers to the ORR on the electrocatalysts were characterized by a rotating disk electrode (RDE) operated in O_2-saturated 0.1 mol L^{-1} $HClO_4$ solution at various rotating rates. As there might be a substantial drop of the diffusion-limiting currents occurred at relatively low loadings,[31,40] the metal loading on the electrode was controlled at 40.5 μg cm^{-2}. As shown in Figure 8, the polarization curves indicate that the ORR occurs under mixed kinetic-diffusion control at the potential region between 0.6 to 1.0 V followed by a plateau of diffusion limiting current depends on the rotating rates below 0.6 V. The number of electrons for the ORR can be estimated by the Koutecky−Levich equation[41]

$$1/i = 1/i_k + 1/(0.62nFC_{O_2}D_{O_2}^{2/3}n^{-1/6}\omega^{1/2}) \quad (2)$$

where i_k is the kinetic current density for the ORR process, i is the measured current density normalized to the geometry surface area of the electrode, n is the number of electrons for the ORR process, F is the Faraday constant, D_{O_2} is the diffusion coefficient, ν is the kinematic viscosity, Co_2 represents the bulk concentration of O_2, and ω is the rotation rate. The kinetic current was calculated based on the following equation

$$i_k = ii_d/(i_d - i) \quad (3)$$

where i_d is the diffusion limiting current. According to the Koutecky−Levich equation, n can be calculated from the slope of i^{-1} plotted against $\omega^{-1/2}$. The following values are referred when calculating the number of electrons transferred: $D_{O_2} = 1.9 \times 10^{-5}$ cm^2 s^{-1},[42] $\nu = 9.87 \times 10^{-3}$ cm^2 s^{-1},[43] $C_{O_2} = 1.18 \times 10^{-6}$ mol cm^{-3}.[44] The corresponding K−L plots are presented in panels b and d in Figure 8, and the n value obtained from the curves are 3.9 for the Pt/HLPC and 4.0 for the Pt/Vulcan XC-

dx.doi.org/10.1021/am403432h | ACS Appl. Mater. Interfaces 2014, 6, 819−825

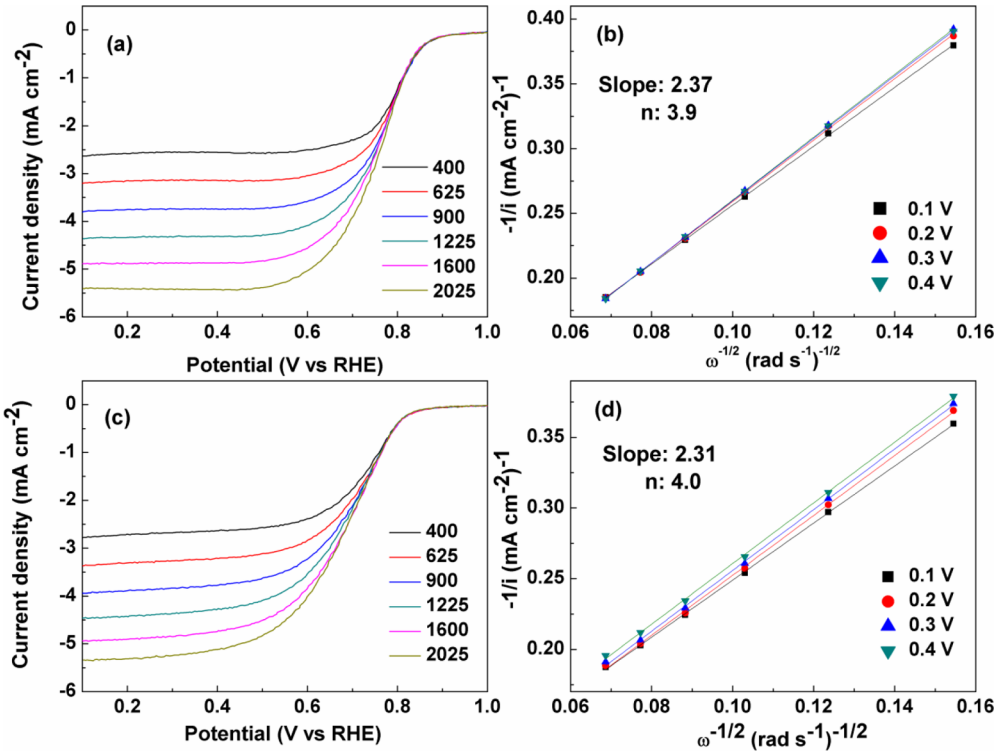

Figure 8. Polarization curves of the (a) Pt/HLPC and (c) Pt/Vulcan XC-72 in 0.1 mol L^{-1} $HClO_4$ solution saturated with O_2 at a scan rate of 5 mV s^{-1} with different rotating speeds, and (b, d) the corresponding Koutecky–Levich plots.

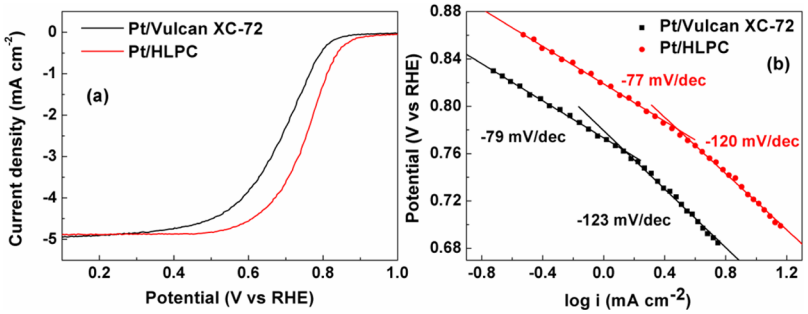

Figure 9. (a) Polarization curves of the Pt/HLPC and Pt/Vulcan XC-72 in 0.1 mol L^{-1} $HClO_4$ solution saturated with O_2 at a scan rate of 5 mV s^{-1} rotated at 1600 rpm and (b) the corresponding Tafel plots.

72. The results suggest that O_2 is reduced through the four-electron reaction with both the electrocatalysts, which is the most efficient pathway[45] and highly favored for practical applications compared with the two-electron reaction.[46]

The polarization curves of the two electrocatalysts recorded at 1600 rpm are shown in Figure 9a. As shown in the curves, the on-set potential of Pt/HLPC is 0.95 V, which is more positive than the Pt/Vulcan XC-72 (0.88 V). The half-wave potential of Pt/HLPC is 0.76 V, which also shifts to the positive potentials compared with the Pt/Vulcan XC-72 (0.69 V). To further analyze the kinetics of the ORR occuring on the surface of the two electrocatalysts, we present the mass-transport corrected Tafel plots of the catalysts in Figure 9b according to the Tafel equation.[47] The Tafel plots exhibit two distinct slopes of −60 mV dec^{-1} and −120 mV dec^{-1} at low and high overpotential ranges were typically reported in the absence of Nafion in the catalyst layer and with ultralow Pt loading, assuming 100 % catalyst utilization.[48] As can be seen, the Tafel plot for Pt/Vulcan XC-72 exhibit two linear regions with the slopes of −79 mV dec^{-1} and −126 mV dec^{-1}, whereas those for Pt/HLPC are −77 mV dec^{-1} and −120 mV dec^{-1}, which are in great accordance with the previous report for the ORR on Pt electrodes.[49] Furthermore, the Tafel slopes for the Pt/HLPC is slightly smaller compared with the Pt/Vulcan XC-72, indicating larger transfer coefficient and enhanced ORR kinetics of Pt/HLPC. The exchange current densities (i_0) of the Pt/HLPC (7.76×10^{-6} mA cm^{-2} for low overpotential and 5.89×10^{-4} mA cm^{-2} for high overpotential) are larger than the Pt/Vulcan XC-72 (1.70×10^{-6} mA cm^{-2} for low overpotential and 2.45×10^{-4} mA cm^{-2} for high overpotential), also suggesting that the Pt/HLPC exhibits better electrocatalytic properties than Pt/Vulcan XC-72.

Figure 10 shows the corresponding mass and specific activity of the two catalysts at various potentials. The mass activity is the ratio between the catalytic oxygen reduction activity (current at a given potential) and the cost (equivalent to the employed mass) of the Pt catalysts,[50] and it is an index to indicate the applicability of the catalyst for ORR.[51] The mass activity can be calculated using the following equation

dx.doi.org/10.1021/am403432h | ACS Appl. Mater. Interfaces 2014, 6, 819−825

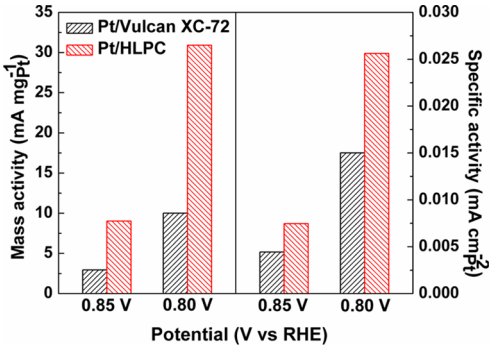

Figure 10. Mass and specific activities of the Pt/Vulcan XC-72 and Pt/HLPC.

$$i_{mass} = iS/m \quad (4)$$

where i_{mass} is the mass current density, representing the mass activity of the electrocatalyst, i is the measured current density exhibited in Figure 9a that was normalized to the geometry surface areas of the electrode, S is the geometry surface area of the electrode, and m represents the mass amount of Pt nanoparticles loaded on the electrode. The Pt/HLPC exhibit mass activities of 9.0 mA mg^{-1} (at 0.85 V) and 30.9 mA mg^{-1} (at 0.80 V), which are almost two times larger than that of Pt/Vulcan XC-72. The catalytic properties are further investigated by calculating the specific activity (kinetic current per unit surface area of catalysts) through normalizing the kinetic current according to the ECSA of the two electrocatalysts. The specific activities were calculated according to the following equation:

$$i_{specific} = iS/(m\mathrm{ECSA}) \quad (5)$$

where $i_{specific}$ is the specific current density, suggesting the specific activity, i is the measured current density exhibited in Figure 9a that was normalized to the geometry surface areas of the electrode, S is the geometry surface area of the electrode, ECSA is electrochemical surface area of the electrocaralysts, and m represents the mass amount of Pt nanoparticles loaded on the electrode. As shown in Figure 10, Pt/HLPC exhibits higher specific activities (0.0075 and 0.0256 mA/cm$^{-2}_{Pt}$) than Pt/Vulcan XC-72 (0.0044 and 0.0150 mA/cm$^{-2}_{Pt}$) at both 0.85 V and 0.80 V respectively, indicating the accelerated and enhanced ORR kinetic with Pt/HLPC as the electrocatalyst. Comparing with the previous literature data relating to applying ordered[52] or nitrogen-doped[53] porous carbons and graphene,[54] the Pt/HLPC exhibited lower overpotential and higher catalytic activities for the ORR. The enhanced performance mainly contributed to the high surface area, functionalized surface state and the unique three-dimensional interconnected structures of the HLPC, which high impove the mass transportation, the electrochemical utilization of the Pt NPs, and the ORR activity.

4. CONCLUSIONS

The HLPC with high BET specific surface area (2730 m^2 g^{-1}) and doped by nitrogen atoms are fabricated by the nature-inspired design from the fish scale, and applied as the support material for the Pt NP electrocatalyst. The Pt NPs are uniformly dispersed on the porous surface of the HLPC with a narrow size distribution and a small average diameter of ca. 2 nm. The extremely small particle size and high dispersion of Pt NPs significantly improve the electrocatalytic activity toward the ORR process. Through the comparion with the Pt/Vulcan XC-72, the obtained Pt/HLPC exhibits larger ECSA, higher oxygen reduction current density and better catalytic activity toward the ORR through the four-electron transfer pathway. The hierarchical lamellar pore structure, large surface area, and functionalized surface state are amenable to promoting the catalytic properties of Pt NPs. Low-cost production, well-developed pore structures, and unique properties of the HLPC make it a promising support material for the ORR electrocatalysts.

AUTHOR INFORMATION

Corresponding Authors

*E-mail: wangf@mail.buct.edu.cn. Phone & Fax: +86 10 64451996.

*E-mail: huangyaqin@mail.buct.edu.cn. Phone: +86 10 64451996.

Author Contributions

†Authors H.L. and Y.C contributed equally to this work.

Notes

The authors declare no competing financial interest.

ACKNOWLEDGMENTS

This work was supported by National Natural Science Funds of China (Grant 51125007) and the National Key Technology R&D Program (2009BAE87B01) from the Ministry of Science and Technology of the People's Republic of China.

REFERENCES

(1) Arroyo-Ramírez, L.; Rodríguez, D.; Otaño, W.; Cabrera, C. R. *ACS Appl. Mater. Interfaces* **2012**, *4*, 2018−2024.
(2) Tang, H.; Peikang, S.; Jiang, S. P.; Wang, F.; Pan, M. *J. Power Sources* **2007**, *170*, 85−92.
(3) Aravind, S. S. J.; Ramaprabhu, S. *ACS Appl. Mater. Interfaces* **2012**, *4*, 3805−3810.
(4) Debe, M. K. *Nature* **2012**, *486*, 43−51.
(5) Rao, C. V.; Viswanathan, B. *J. Phys. Chem. C* **2009**, *113*, 18907−18913.
(6) Kadirgan, F.; Kannan, A. M.; Atilan, T.; Beyhan, S.; Ozenler, S. S.; Suzer, S.; Yörür, A. *Int. J. Hydrogen Energy* **2009**, *34*, 9450−9460.
(7) Chen, Y.; Liang, Z.; Yang, F.; Liu, Y.; Chen, S. *J. Phys. Chem. C* **2011**, *115*, 24073−24079.
(8) Tang, S. H.; Sun, G. Q.; Qi, J.; Sun, S. G.; Guo, J. S.; Xin, Q. *Chin. J. Catal.* **2010**, *31*, 12−17.
(9) Qiao, Y.; Li, C. M. *J. Mater. Chem.* **2011**, *21*, 4027−4036.
(10) Winter, M.; Brodd, R. J. *Chem. Rev.* **2004**, *104*, 4245−4270.
(11) Liu, H.; Li, J.; Xu, X.; Wang, F.; Liu, J.; Li, Z.; Ji, J. *Electrochim. Acta* **2013**, *93*, 25−31.
(12) Wen, Z. H.; Wang, Q.; Li, J. H. *Adv. Funct. Mater.* **2008**, *18*, 959−964.
(13) Huang, J.; Hou, H.; You, T. *Electrochem. Commun.* **2009**, *11*, 1281−1284.
(14) Oh, J.; Lee, C.; Kim, H. *Electrochem. Commun.* **2007**, *9*, 2629−2632.
(15) Basova, Y. V.; Hatori, H.; Yamada, Y.; Miyashita, K. *Electrochem. Commun.* **1999**, *1*, 540−544.
(16) Matter, P. H.; Zhang, L.; Ozkan, U. S. *J. Catal.* **2006**, *239*, 83−96.
(17) Kuo, P. L.; Hsu, C. H.; Li, W. T.; Jhan, J. Y.; Chen, W. F. *J. Power Sources* **2010**, *195*, 7983−7990.
(18) Wen, Z. H.; Liu, J.; Li, J. H. *Adv. Mater.* **2008**, *20*, 743−747.
(19) Su, F.; Tian, Z.; Poh, C. *Chem. Mater.* **2010**, *22*, 832−839.
(20) Chen, W.; Zhang, H.; Huang, Y. *J. Mater. Chem.* **2010**, *20*, 4773−4775.
(21) Liu, Z.; Guo, F.; Hong, L.; Lim, T.H. *Electrochem.Commun.* **2006**, *8*, 83−90.

(22) Liu, Z.; Lee, J. Y.; Chen, W.; Han, M.; Gan, L. M. *Langmuir* **2004**, *20* (1), 181−187.
(23) Wang, Z.; Li, F.; Ergang, N.; Stein, A. *Chem. Mater.* **2006**, *18*, 5543−5553.
(24) Yamada, H.; Moriguchi, I.; Kudo, T. *J. Power Sources* **2008**, *175*, 651−656.
(25) Wang, H.; Maiyalagan, T.; Wang, X. *ACS Catal.* **2012**, *2*, 781−794.
(26) Lyth, S. M.; Nabae, Y.; Moriya, S.; Kuroki, S.; Kakimoto, M.; Ozaki, J.; Miyata, S. *J. Phys. Chem. C* **2009**, *113*, 20148−20151.
(27) Ikeda, S.; Tachi, K.; Ng, Y. H.; Ikoma, Y.; Sakata, T.; Mori, H. *Chem. Mater.* **2007**, *19*, 4335−4340.
(28) Biniak, S.; Szymanski, G.; Siedlewski, J.; Swiatkowski, A. *Carbon* **1997**, *35* (12), 1799−17810.
(29) Piñero, E.; Cadek, M.; Béguin, F. *Adv. Funct. Mater.* **2009**, *19*, 1032−1039.
(30) Zhang, X.; Chan, K. Y. *Chem. Mater.* **2003**, *15*, 451−459.
(31) Lim, B.; Jiang, M.; Camargo, P.H.C.; Cho, E.C.; Tao, J.; Lu, X.; Zhu, Y.; Xia, Y. *Science* **2009**, *324*, 1302−1305.
(32) Pozio, A.; De Francesco, M.; Cemmi, A.; Cardellini, F.; Giorgi, L. *J. Power Sources* **2002**, *105*, 13−19.
(33) Schmidt, T. J.; Gasteiger, H. A.; Stäb, G. D.; Urban, P. M.; Kolb, D. M. *J. Electrochem. Soc.* **1998**, *145*, 2354−2358.
(34) Suryamas, A. B.; Anilkumar, G. M.; Sago, S.; Ogi, T.; Okuyama, K. *Catal. Commun.* **2013**, *33*, 11−14.
(35) Joo, S. H.; Lee, H. I.; You, D. J.; Kwon, K.; Kim, J. H.; Choi, Y. S.; Kang, M.; Kim, J. M.; Pak, C.; Chang, H.; Seung, D. *Carbon* **2008**, *46*, 2034−2045.
(36) Kim, D.; Abo Zeid, E. F.; Kim, Y. *Electrochim. Acta* **2010**, *55*, 3628−3633.
(37) Schmidt, T. J.; Gasteiger, H. A.; Stab, G. D.; Urban, P. M.; Kolb, D. M.; Behm, R. *J. Electrochem. Soc.* **1998**, *145*, 2354−2358.
(38) Yun, Y. S.; Kim, D.; Park, H. H.; Tak, Y.; Jin, H. J. *Synth. Met.* **2012**, *162*, 2337−2341.
(39) Shao, Y.; Yin, G.; Gao, Y.; Shi, P. *J. Electrochem. Soc.* **2006**, *153*, A1093−A1097.
(40) Mayrhofer, K. J. J.; Strmcnik, D.; Blizanac, B. B.; Stamenkovic, V.; Arenz, M.; Markovic, N. M. *Electrochim. Acta* **2008**, *53*, 3181−3188.
(41) Kondo, S.; Nakamura, M.; Maki, N.; Hoshi, N. *J. Phys. Chem. C* **2009**, *113*, 12625−12628.
(42) Zečević, S. K.; Wainright, J. S.; Litt, M. H.; Gojković, S. L.; Savinell, R. F. *J. Electrochem. Soc.* **1997**, *144*, 2973−2982.
(43) Mello, R. M. Q.; Ticianelli, E. A. *Electrochim. Acta* **1997**, *42*, 1031−1039.
(44) Chen, W.; Kim, J.; Sun, S.; Chen, S. *J. Phys. Chem. C* **2008**, *112*, 3891−3898.
(45) Wang, B. *J. Power Sources* **2005**, *152*, 1−15.
(46) Sepa, D. B.; Vojnovic, M. V.; Vracar, L. M.; Damjanovic, A. *Electrochim. Acta* **1986**, *31*, 91−96.
(47) Pino, L.; Vita, A.; Corfaro, M.; Recupero, V.; Hegde, M. S. *Appl. Catal. A* **2003**, *243*, 135−146.
(48) Seidel, Y. E.; Schneider, A.; Jusys, Z.; Wickman, B.; Kasemo, B.; Behm, R. J. *Faraday Discuss.* **2009**, *140*, 167−184.
(49) Chen, Z.; Higgins, D.; Tao, H.; Hsu, R. S.; Chen, Z. *J. Phys. Chem. C* **2009**, *113*, 21008−21013.
(50) Gasteiger, H. A.; Kocha, S. S.; Sompalli, B.; Frederick, T. W. *Appl. Catal., B* **2005**, *56*, 9−35.
(51) Hwang, B. J.; Kumar, S.; Chen, C.; Cheng, M.; Liu, D.; Lee, J. *J. Phys. Chem. C* **2007**, *111*, 15267−15276.
(52) Su, F.; Poh, C. K.; Tian, Z.; Xu, G.; Koh, G.; Wang, Z.; Liu, Z.; Lin, J. *Energy Fuels* **2010**, *24*, 3727−3732.
(53) Su, F.; Tian, Z.; Poh, C. K.; Wang, Z.; Lim, S. H.; Liu, Z.; Lin, J. *Chem. Mater.* **2010**, *22*, 832−839.
(54) Kou, R.; Shao, Y.; Wang, D.; Engelhard, M. H.; Kwak, J. H.; Wang, J.; Viswanathan, V. V.; Wang, C.; Lin, Y.; Wang, Y.; Aksay, I. *Electrochem. Commun.* **2009**, *11* (5), 954−957.